Optical actuation of microelectromechanical systems using photoelectrowetting

Matthieu Gaudet, S. Arscott

Optical actuation of microelectromechanical systems using photoelectrowetting

Cite as: Appl. Phys. Lett. **100**, 224103 (2012); https://doi.org/10.1063/1.4723569
Submitted: 13 January 2012 • Accepted: 14 May 2012 • Published Online: 31 May 2012

Matthieu Gaudet and Steve Arscott

Optical actuation of microelectromechanical systems using photoelectrowetting

Matthieu Gaudet and Steve Arscott[a)]
Institut d'Electronique, de Microélectronique et de Nanotechnologie (IEMN), CNRS UMR8520, The University of Lille, Cité Scientifique, Avenue Poincaré, 59652 Villeneuve d'Ascq, France

(Received 13 January 2012; accepted 14 May 2012; published online 31 May 2012)

We demonstrate a proof-of-concept that microelectromechanical systems (MEMS) can be optically actuated using photoelectrowetting. A 30 μm thick aluminium cantilever is actuated using an ordinary white light source via the modulation of capillary forces in a liquid bridge on a Teflon® coated commercial silicon wafer. A deflection of 58 μm is observed using a light power of 100 mW at a bias of 7 V. The deflection of the cantilever relies on the photoelectrowetting effect [S. Arscott, Sci. Rep. **1**, 184 (2011)]. Such wireless actuation could be useful for optical addressing and control of autonomous wireless sensors, MEMS, and microsystems. © *2012 American Institute of Physics*. [http://dx.doi.org/10.1063/1.4723569]

Microelectromechanical systems (MEMS) now have numerous applications in terms of sensors and actuators.[1] MEMS are commonly actuated[1] piezoelectrically, electrostatically, and thermally but also using techniques such as electrowetting.[2–4] Wireless optical actuation currently relies on radiation pressure[5–9] and photomechanical layers based on nanowires[10] and shape memory.[11] We demonstrate here a proof-of-concept that MEMS can be actuated using an ordinary white light source via the photoelectrowetting effect.[12] Wireless actuation, based on a physical effect, could be advantageous for optical addressing and control of autonomous wireless sensors,[13] which currently rely on a complex circuit-based systems approach,[14] and also autonomous microsystems which are currently under development.[4,15]

In contrast to using a photoconductor[16] to control electrowetting,[17,18] the photoelectrowetting effect relies on the voltage and optical modulation of the space-charge region of a semiconductor in a liquid/insulator/semiconductor (LIS) junction. Let us consider Fig. 1(a), which shows a droplet resting on an insulator/semiconductor stack. If the semiconductor is grounded, then at 0 V the droplet will form a contact angle θ_0 with that surface. In the case of p-type semiconductor, placing the droplet to a potential $+V$ will create a depletion region having a depth $d_s(V,0)$ in the semiconductor. The voltage induced decrease in the capacitance (per unit area) leads to a modification of the contact angle of the droplet on the surface to $\theta_{V,0}$ [see Fig. 1(b)]. Note that $\theta_{V,0} \neq \theta_{-V,0}$; this is known as *asymmetrical-electrowetting-on-semiconductors*.[12] Irradiation of the semiconductor by above-band gap photons generate electron-hole pairs that modify the depth of the depletion region to $d_s(V,I)$. The effect of this is a decrease of the value of the contact angle to $\theta_{V,I}$ [Fig. 1(c)]; this is known as *photoelectrowetting-on-semiconductors*.[12]

The photoelectrowetting effect can be directly interpreted by a modification of the Young-Lippmann[17] equation in the following way,

$$\cos\theta_{V,I} = \cos\theta_0 + \frac{1}{2\gamma} C_{V,I} V^2, \tag{1}$$

where $\theta_{V,I}$ is the contact angle which depends on the voltage V and the light irradiance I, θ_0 is the contact angle at zero bias, γ is the surface tension of the liquid. The voltage and light dependent areal capacitance $C_{V,I}$ is given by

$$C_{V,I} = \frac{\varepsilon_i \varepsilon_s \varepsilon_0}{d_s(V,I)\varepsilon_i + d_i \varepsilon_s}, \tag{2}$$

where ε_i and ε_s are the dielectric constants of the insulator and the semiconductor and d_i and $d_s(V,I)$ are the insulator thickness and the voltage and light dependent thickness of the space-charge layer in the semiconductor respectively. For an LIS junction, both electrowetting and photoelectrowetting will depend upon both semiconductor doping type and density.[12] In classic electrowetting, a $\cos\theta \propto V^2$ relationship is observed.[17] In contrast, for a reverse bias LIS junction, $\cos\theta$ is not proportional to V^2.[12]

Let us now consider Fig. 2 which shows a droplet of conducting liquid resting on an insulator/semiconductor stack. The droplet is also in contact with a microcantilever which has a stiffness k, length l, width w, and thickness t. In terms of the forces applied by the droplet to the rest of the system, the following forces have to be considered:[19] The surface tension force F_{st} acting at the contact line on the cantilever and the capillary pressure force F_{cp} due to the

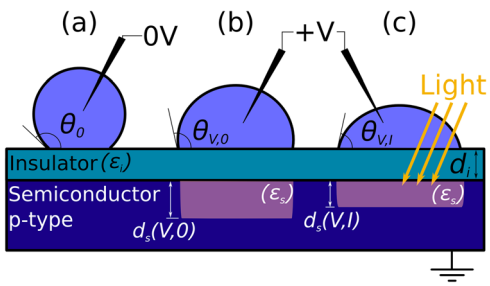

FIG. 1. Electrowetting-on-semiconductors and photoelectrowetting on semiconductors.

[a)]steve.arscott@iemn.univ-lille1.fr.

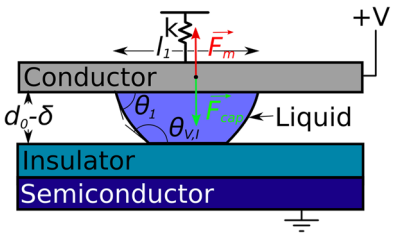

FIG. 2. Balance of capillary forces and mechanical restoring force of a cantilever for a droplet between two surfaces.

pressure difference ΔP across the curved liquid-air interface ($\Delta P = P_{inside} - P_{outside} = 2\gamma H$ where the mean curvature $H = {}^1/_2(\kappa_1 + \kappa_2)$; κ_1 and κ_2 are the principle curvatures). The total capillary force F_{cap} can be written as

$$F_{cap} = 2\gamma \sin\theta_1 (l_1 + w) - w l_1 \gamma \left(\kappa_1 - \frac{\cos\theta_1 + \cos\theta_{V,I}}{d_0 - \delta} \right), \tag{3}$$

where θ_1 is the contact angle on the cantilever surface and $\theta_{V,I,}$ the contact angle on the insulator/silicon surface depending of the voltage V and the irradiance I, d_0 is the initial distance between the plates, δ is the vertical displacement of the cantilever, the liquid wets the conducting surface over a length l_1 and κ_1 is the positive curvature of the liquid/air interface considered at the contact line on the cantilever. F_{st} is always positive (acting downwards) but F_{cp} can be positive or negative depending on the magnitude and *sign* of κ_2; the minus signs in Eq. (3) account for this.

In equilibrium, we can consider that mechanical restoring force of the cantilever $F_m = F_{cap}$. If we consider the capillary force to be acting at a point $a = l\text{-}(l_1/2)$ from the end of the cantilever F_m can be written as follows:[20]

$$F_m = \frac{\delta E w t^3}{2a^2(3l - a)}, \tag{4}$$

where E is the Young's modulus of the cantilever.

In order to conduct experiments Teflon®AF 1600 (Dupont, USA) coated commercial single crystal silicon wafers (Siltronix, France) were prepared. The Teflon/silicon stacks were composed of 20 nm (±3 nm) and 265 nm (±15nm) thick Teflon layers which had been spin-coated (the processing parameters can be found elsewhere[12]) onto p-type ($N_A \sim 1.8 \times 10^{15}\,cm^{-3}$) and n-type ($N_A \sim 6 \times 10^{14}\,cm^{-3}$) silicon wafers. An Al based ohmic contact was formed on the rear surface of the silicon wafer to provide an electrical contact. Fig. 3 shows the variation of the contact angle of a sessile droplet with incident light on a 265 nm Teflon coated p-type silicon wafer. The white light source was a KL2500 LCD (Schott, Germany) using a 13163 type halogen lamp (Philips, NL) which was calibrated using a 210 Power Meter (Coherent, USA). As the lamp power is increased from 0 to 50 mW, the contact angle of the droplet reduces as predicted by Eq. (1) due to the electron-hole generation rate g which depends on the irradiance and agrees well with a proposed model.[12] The photoelectrowetting effect allows the contact angle to be varied in a continuous way. The data was gathered using a commercial Contact

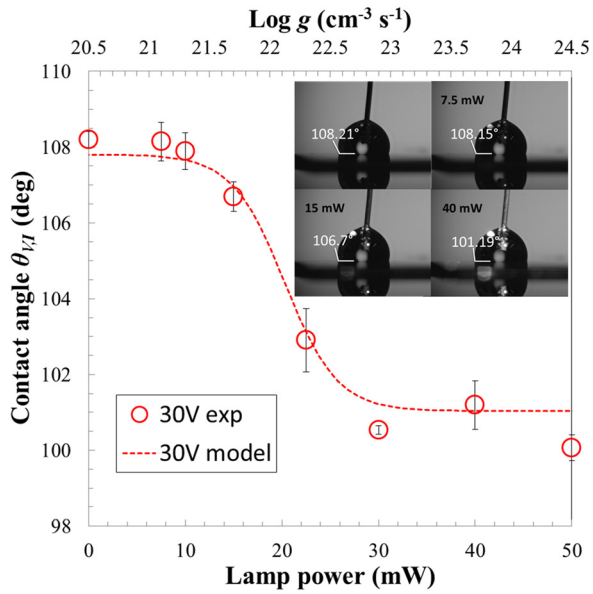

FIG. 3. Variation of contact angle with illumination of a sessile droplet (H_2O/HCl, 0.01 M) on a Teflon (265 nm) coated p-type silicon wafer ($N_A = 1.8 \times 10^{15}\,cm^{-3}$) measured at +30 V (open red circles). Modelled curve (dashed red line) based on electron-hole generation in depletion region, see Ref. 12. Inset shows variation of droplet profile.

Angle Meter (GBX Scientific Instruments, France) and the experiments were performed in a class ISO 5/7 cleanroom ($T = 20\,°C \pm 0.5\,°C$; $RH = 45\% \pm 2\%$). Contact angles are extracted using an active contour approach.[21] The response time of the droplet (to light) is ~70 ms.

We subsequently implemented the simple microcantilever set-up shown in Fig. 4. Aluminium cantilevers having a thickness of 30 μm were mounted on a glass support wafer. Taking the Young's modulus of Al to be 70 GPa, the spring constant of the cantilevers is calculated to be 1.3 Nm^{-1} (p-type data) and 1.9 Nm^{-1} (n-type data). A volume (5-10 μl) of HCL (solution conductivity = 3.64 m Scm^{-1}) is placed between the cantilever and the Teflon surface. The calibrated white light source was used to illuminate the samples (the sample was illuminated with the output of the light source at ≈10° angle with respect to the wafer surface and at a distance of ~10 mm from the cantilever). For p-type (n-type) silicon, a positive (negative) voltage is applied to the aluminium in order to deplete the silicon at the Teflon/silicon interface. In this way, the droplet spreads out according to Eq. (1) with the thickness of the depletion layer d_s modified by voltage and light.[12] According to Eqs. (3) and (4), the variation of the contact angle generates a deflection of the cantilever. Fig. 5

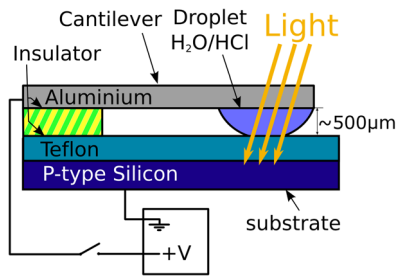

FIG. 4. Experimental setup showing aluminium cantilever, liquid (H_2O/HCl, 0.01 M) and Teflon AF/silicon photoelectrowetting surface.

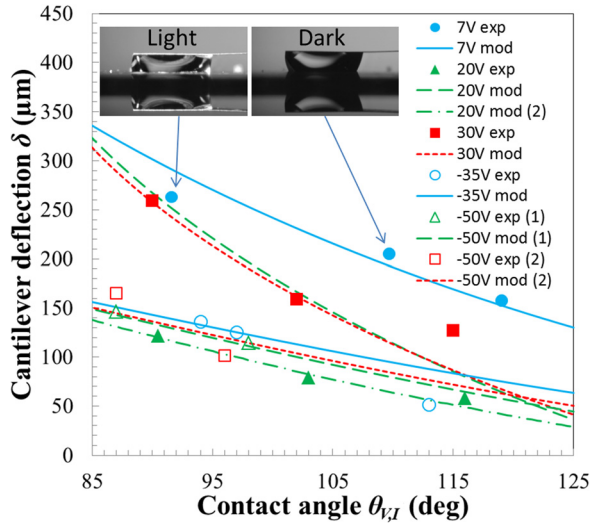

FIG. 5. Variation of cantilever deflection with contact angle on the Teflon coated p-type (filled shapes) and n-type (open shapes) silicon wafers. Teflon thickness = 265 nm except "7 V exp" data (20 nm). Cantilever dimensions for p-type (n-type): $l = 9$ mm, $w = 3$ mm, $t = 30\,\mu$m ($l = 8.5$ mm, $w = 2.5$ mm, $t = 30\,\mu$m). Lamp power = 100 mW except "20 V exp" data (65 mW) and "50 V(2) exp" data (240 mW). Liquid = H_2O/HCl (0.01 M) except "−35V exp" data (deionized water). Curves correspond to model based on Eqs. (3) and (4). The inset shows the optical actuation of the cantilever at 7 V.

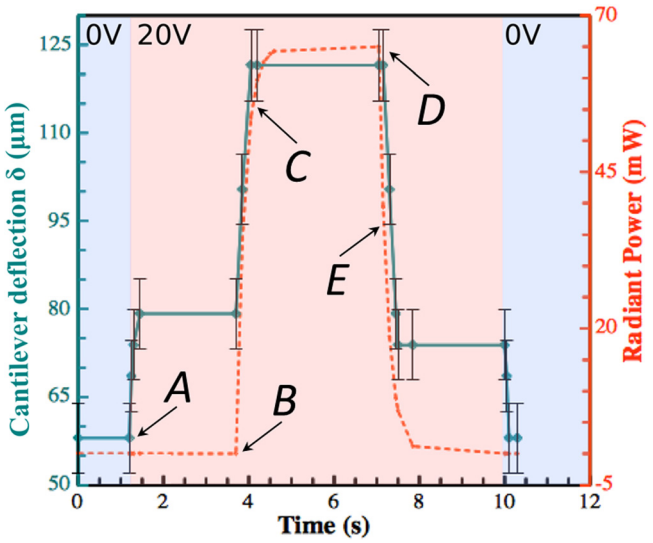

FIG. 6. Evolution of the cantilever displacement (solid curve) with time for applied voltage and illumination using a Teflon AF (265 nm)/p-type silicon ($N_A = 1.8 \times 10^{15}\,\text{cm}^{-3}$) stack. The dashed curve corresponds to the lamp power.

shows the cantilever deflection as a function of contact angle on the Teflon surface under (i) zero-bias, (ii) reverse bias/non-illuminated, and (iii) reverse bias/illuminated conditions. The modelled curves are obtained equating Eqs. (3) and (4) and solving the resulting quadratic equation. We consider κ_I to be constant; we use $250\,\text{m}^{-1}$ (p-type data) and $714\,\text{m}^{-1}$ (n-type data). We also consider θ_I to be constant at 82.2°. The following experimental values are used to generate the curves in Fig. 5: $\theta_I = 82.2°$, "7 V model" ($l_I = 3.02$ mm, $d_0 = 930\,\mu$m), "20 V model" ($l_I = 5.21$ mm, $d_0 = 830\,\mu$m), "30 V model" ($l_I = 2.94$ mm, $d_0 = 608\,\mu$m), "−35V model" ($l_I = 2.3$ mm, $d_0 = 1300\,\mu$m), "−50 V model (1)" ($l_I = 2.82$ mm, $d_0 = 1310\,\mu$m) and "−50 V model (2)" ($l_I = 2.72$ mm, $d_0 = 1340\,\mu$m). The experiment data is in good agreement with the modelled curves except the "20 V exp" data (filled triangles); in this case Eq. (4) may not be valid as l_I is large. However, if we consider the force is applied at l-l_I the data can be fitted (see "20 V model (2)" dash-dot green line in Fig. 5). Optically stimulated deflections of 58 μm and 101 μm were observed for 20 nm and 265 nm Teflon/p-type silicon samples at 7 V and 30 V (see Table I). The lower deflections on the n-type material are due to a stiffer cantilever and larger d_0; the latter has the effect of reducing the capillary force. The process is reversible; switching off the light returns the cantilever to the non-illuminated position.

TABLE I. Summary of the optically actuated cantilever deflection $\delta_{V,I}$ values.

Experiment	$\delta_{V,I}$ (μm)
7 V exp	58
20 V exp	43
30 V exp	101
−35V exp	11
−50V exp (1)	32
−50 V exp (2)	63

Fig. 6 shows the evolution of the cantilever deflection with time for applied voltage and light. The deflection values reported on the graph are extracted from the images of the experimental film (time interval between two images = 50 ms). The y-axis error bars reported on the graph correspond to the variation of half a pixel on the analysed images. At $t = 0$ s, the droplet is placed between the Teflon surface and the aluminium cantilever which generates a deflection of the cantilever of 58 μm at 0 V. At $t = 1.15$ s (point A), the voltage is stepped to +20 V. The variation of $\theta_{V,I}$ generates a deflection of the cantilever to 79 μm. At $t = 3.65$ s, the lamp is turned on (point B). The light irradiance follows an exponential with a time constant being measured at the value $\tau_{lamp} = 200$ ms. After 50 ms and during the next 350 ms, the deflection of the cantilever evolves to stabilize at the value of 122 μm. At this instant, the radiant power of the lamp is 53.3 mW (point C) and continues evolving to achieve its maximum at $t = 4.6$ s. At $t = 7.05$ s, the lamp is turned off (point D). The radiant power decreases with a time constant being measure to be τ_{lamp}. After 100 ms, the radiant power has a value of 39 mW (point E). The deflection of the cantilever decrease to 73 μm over a time of 450 ms.

For a lamp power higher than 53.3 mW, i.e., 82% of the full radiant power, the non-displacement of the cantilever is explained by the saturation of the electron-hole generation phenomenon.[22] This saturation is also observable during the decrease of the radiant power, having an effect on the cantilever deflection for a value lower than 39 mW, i.e., 60% of the full radiant power. The non-symmetrical variation of the radiant power having an effect of the cantilever deflection during the increase (point C) and the decrease (point E) phase of the radiant power can be explained by the time step of 50 ms generating an x-axis error of each point of the deflection curve. The time error gives an error of 5% on the radiant power when the light is turned on and a 17% when

the lamp is turned off, according to the position of the point along the exponential curves; these values correspond to saturation for a radiant power of 40-50 mW, cf. Fig. 3.

Finally, it should be noted that actuation using a liquid/insulator/semiconductor junction ensures low power consumption actuation in a similar way as the MOS junction[22] provides a low power device as actuation is achieved at virtually zero current. By demonstrating an overlap between MEMS, wetting phenomena and semiconductors we have shown here that silicon-based technologies incorporating these three subjects are feasible.

[1]J. Bryzek, S. Roundy, B. Bircumshaw, C. Chung, K. Castellino, J. R. Stetter, and M. Vestel, IEEE Circuits Devices Mag. **22**, 8 (2006).
[2]J. Lee and C.-J. Kim, J. Micromech. Syst. **9**, 171 (2000).
[3]I. Moon and J. Kim, Sens. Actuators A **130–131**, 537 (2006).
[4]Y. Mita, Y. Li, M. Kubota, S. Morishita, W. Parkes, L. I. Haworth, B.W. Flynn, J. G. Terry, T.-B. Tang, A. D. Ruthven, S. Smith, and A. J. Walton, Solid-State Electron. **53**, 798 (2009).
[5]A. Ashkin and J. M. Dziedzic, Appl. Phys. Lett. **19**, 283 (1971).
[6]R. C. Gauthier, R. Tait, H. Mende, and C. Paulowicz, Appl. Opt. **40**, 930 (2001).
[7]M. Sulfridge, T. Saif, N. Miller, and K. O'Hara, J. Microelectromech. Syst. **11**, 574 (2002).
[8]S. Pal and A. K. Ghosh, Electron. Lett. **42**, 580 (2006).
[9]T. Carmon, H. Rokhsari, L. Yang, T. J. Kippenberg, and K. J. Vahala, Phys. Rev. Lett. **94**, 223902 (2005).
[10]S. V. Ahir and E. M. Terentjev, Nature Mater. **4**, 491 (2005).
[11]A. Lendlein, H. Jiang, O. Jünger, and R. Langer, Nature **434**, 879 (2005).
[12]S. Arscott, Sci. Rep. **1**, 184 (2011).
[13]J. M. Kahn, R. H. Katz, and K. S. J. Pister, in *Proceedings of ACM MobiCom'99*, Washington, DC, 1999, p. 271.
[14]J. Yick, B. Mukherjee, and D. Ghosal, Comput. Netw. **52**, 2292 (2008).
[15]R. J. Wood, IEEE Trans. Rob. **24**, 341 (2008).
[16]S.-Y. Park, M. A. Teitell, and P. Y. Chiou, Lab Chip **10**, 1655 (2010).
[17]F. Mugele and J.-C. Baret, J. Phys. Condensed Matter. **17**, R705 (2005).
[18]A. R. Wheeler, Science **322**, 539 (2008).
[19]M. A. Fortes, J. Colloid. Interface Sci. **88**, 338 (1982).
[20]W. C. Young and R. G. Budynas, *Roark's Formulas for Stress and Strain*, 7th ed. (McGraw-Hill, New York, 2002), p. 189.
[21]A. F. Stalder, G. Kulik, D. Sage, L. Barbieri, and P. Hoffmann, Colloids Surf. A **286**, 92 (2006).
[22]S. M. Sze and K. K. Ng, *Physics of Semiconductor Devices*, 3rd ed. (Wiley, New Jersey, 2007).